Improving UV Resistance of Fibers: Idealized Computational Model Predicting the Distribution of UV Blocking Cylindrical Nanoparticles in Protective Polymeric Layer

Abdelfattah Mohamed Seyam, PhD, Rahul Vallabh, PhD, Ahmed H. Hassanin, PhD

North Carolina State University, Raleigh, NC UNITED STATES

Correspondence to:
Abdelfattah Mohamed Seyam email: aseyam@tx.ncsu.edu

ABSTRACT

High strength fibers such as PBO and Kevlar are used to produce composites, bulletproof vests, tendons of giant scientific balloons, and other high performance products. These fibers, however, are known to degrade upon exposure to Ultraviolet (UV) radiation which causes premature failure of the end-products. Improving UV resistance of high strength fibers like PBO through methods such as adding UV inhibiting particles during filament spinning or dyeing/coating process is not only extremely difficult, but often fails to provide the adequate UV protection. As an alternative to conventional approaches, UV protection of high performance yarns/braids can be effectively achieved by covering them with a polymeric sheath containing dispersed UV inhibiting nanoparticles. In this work, a computational model was developed to optimize critical factors such as thickness (weight) of the protective sheath and the amount of UV blockers for a given particle size, which influence the UV protective efficiency of the sheath. In order to simulate three-dimensional dispersion of nanoparticles in a polymer matrix, the model considers a random distribution of cylindrical nanoparticles of different size, aspect ratio, and volume fraction in a three-dimensional volume of protective sheath of a given length, width, and thickness. 2D visualization and image analysis techniques were utilized to determine the area projected by the particles on the x-y plane (areal coverage provided by nanoparticles). The areal coverage values obtained from the model were found to be higher than the experimental results due to the agglomeration of nanoparticles in the sheath caused during the polymer compounding process. However, the purpose of the model is to serve as a benchmarking tool to aid in the design and development of UV protective sheaths and films, and not to estimate absolute UV protection values. Analysis of the relationship between areal coverage and various input parameters in the model show that areal coverage increases with an increase in particle volume fraction and film thickness, and a decrease in particle diameter and length. It was also found that areal coverage was more significantly influenced by particle aspect ratio than by particle length.

Keywords: High Performance Fiber; UV Blocker; Nanoparticles; Computational Model; Areal coverage; UV Protective Layer; Scientific Balloons

INTRODUCTION

In general, textile fibers are prone to degradation by Ultraviolet (UV) radiations and there is a continued interest in research associated with UV protection of textile materials [1-16]. Exposure to UV radiations results in destructive and damaging effects like mass loss, deterioration in the mechanical properties, color changes, and change in morphology and structure of surface layer [2, 3]. The energy of the photons in UV radiations breaks chemical bonds resulting in the formation of free radicals that initiate the photo-oxidation [1]. Improving UV resistance of high performance fibers using conventional methods such as adding UV inhibitor to the fibers during the spinning process and dyeing with UV protective materials is extremely difficult. Spinning processes for most high performance fibers involves use of strong acid solvents [14], which makes it difficult to add UV inhibitors during spinning. Dyeability of high performance fibers is also poor because of their highly oriented and packed crystalline structure, and thermal stability [15]. These challenges associated with using conventional methods have prompted researchers to develop an alternative approach involving covering the textile structures like yarns and braids with a protective polymeric sheath (film) containing UV inhibitors (UV absorber and/or blockers), which absorb as well as scatter the UV radiation [4-16].

While many studies have focused on the development of UV protective films/sheaths, no model has been developed to optimize the sheath thickness and the amount of UV particles which are critical in maximizing the UV protection while keeping the sheath weight low. Such a model would serve as a valuable tool for the design and development of UV protective film/sheath. The idealized model developed in this study predicts the protection level (based on the areal coverage provided by nanoparticles) as a function of nanoparticle size, volume fraction of the particles, and protective layer thickness. As the area covered by particles (calculated as the area projected by particles on the plane perpendicular to film thickness direction) increases, the line-of-sight in the thickness direction decreases, thus reducing UV transmittance. The protection level, therefore, is expected to increase with the area covered by particles.

MODEL

Cylindrical nanoparticles are one of the most commonly available shapes and are widely used in many applications due to their high surface area. This model predicts the protection level as a function of nanoparticle size (length and diameter of the cylindrical particles), volume fraction of the particles in the polymer matrix, and protective sheath thickness. In order to reduce complexity and computing time, the following assumptions were made:

1. All particles are cylindrical having identical size (same length and diameter)
2. Particles are randomly distributed in the protective layer (film); i.e. Van der Waals forces are neglected
3. The thickness of the protective layer is uniform

Cylindrical UV blocker nanoparticles available in the market, including those used for preparing film samples in this study, have a narrow size distribution and hence the first assumption would have negligible contribution to any error in the model. With current film forming techniques, it is possible to produce films with minimum thickness variation. Thus, any errors resulting due the third assumption is also expected to be negligible. Nano-scale particles tend to agglomerate due to high Van der Waals forces, however the second assumption is valid in the case of the idealized model developed in this study. The results obtained from the idealized model serve as a benchmark for the degree of dispersion against which degrees of dispersion of nanoparticles in a film or a sheath can be evaluated. It is also important to mention that more research is needed to study the dispersion of nanoparticles. The input parameters of the model are size of UV protective particle (length and diameter), volume fraction of the particles (defined as the ratio of the volume of the particles to the total volume of the protective sheath), and protective film/sheath thickness.

A geometric model to represent nonwoven fabric has been developed in one of our previous studies [17]. A similar approach was used in this study. MATLAB and Visualization Tool Kit (VTK) programs were developed for the computation and visualization of particle dispersion in a polymer matrix. The number of particles (required as an input for the MATLAB program) was calculated from particle diameter and volume fraction of the particles using Eq. (1) and Eq. (2).

$$N = \frac{abcV_f}{V_P} \tag{1}$$

Where
N = number of UV protective particles (cylinders)
a = length of film (computational region)
b = width of film (computational region)
c = thickness film (computational region)
V_f = volume fraction of UV particles
V_p = volume of one particle (cylinder)

$$V_p = \frac{\pi d^2 L}{4} \tag{2}$$

Where
d = particle diameter
L = particle length

The random position (center point xi, yi, zi) for each particle (within the computational region matrix or film holding the particles) was generated using the following functions and conditions in the MATLAB program.

$x_i = rand\ (l)$ $\quad 0 \leq l \leq a$
$y_i = rand\ (n)$ $\quad 0 \leq n \leq b$
$z_i = rand\ (m)$ $\quad 0 \leq m \leq c$

Where "*rand*" is the random function generator and i is the i^{th} position of the particle center point that ranges from 1 to N. The *x-*, *y-*, and *z-axis* are along the length (a), width (b), and thickness (c) of the computational region. The position of each cylindrical particle was decided by its center points while the location of the cylinder was determined by two randomly determined rotational angles (α *and* δ)

around x- and z-axis, respectively (*Figure 1*). The two angles (α, δ) were determined using the following functions and conditions:

$$\alpha_i = \text{rand}(j) \quad 0^\circ \leq j \leq 180^\circ$$
$$\delta_i = \text{rand}(k) \quad 0^\circ \leq k \leq 180^\circ$$

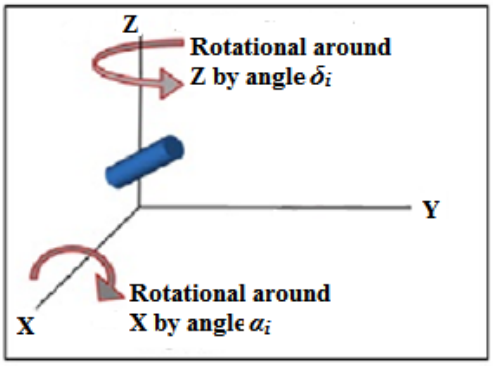

FIGURE 1. Rotation of cylindrical particle around x- and z-axes.

The random positions and orientations of particles generated using MATLAB were exported to a text file and then the text file was input to a VTK (Visualization Tool Kit) program to create final visualizations of the particles dispersed in the computational domain. *Figure 2* shows examples of 2D (right) and 3D (left) visualizations generated by the model. Areal coverage percent was calculated by determining the total white area in the 2D visualization image (using MATLAB function *'bwarea'*) as a percent of the area of the entire image.

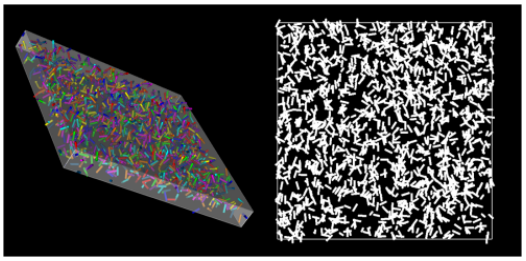

FIGURE 2. 3D visualization (left) and 2D visualization (right).

NUMERICAL RESULTS

Domain Size and Replicability

In order to determine the optimum domain size of the square computational area, two sets of simulations were run with domain size ranging from 500 nm x 500 nm to 2000 nm x 2000 nm. Since the domain size is more likely to influence the areal coverage in the case of smaller number of particles, *N*, the simulations with the lowest number of particles were chosen for this analysis. The first set (A) was run for film thickness of 50 nm while the second set (B) was run for film thickness of 100 nm. Both sets involved cylindrical particles of 15 nm diameter and 60 nm length with the particle volume fraction of 0.03. As seen in *Figure 3*, there is a marginal increase in areal coverage when the domain size is increased from 500 nm x 500 nm to 1000 nm x 1000 nm. Areal coverage remained relatively the same for domain sizes larger than 1000 nm x 1000 nm. Domain size of 1000 nm x 1000 nm was therefore chosen for all simulations for the parametric analysis.

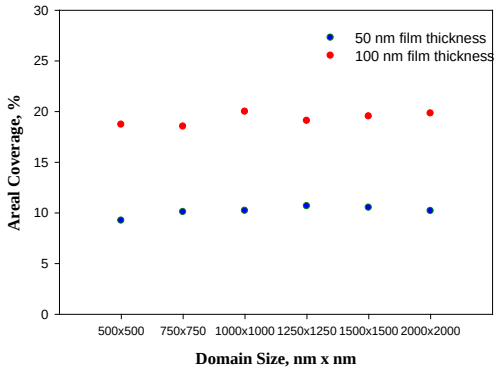

FIGURE 3 Analysis of domain size of the computational area.

To investigate the reproducibility of the simulation results, multiple runs of simulations were run with the same parameter values. Simulation set (C) was run for film thickness of 50 nm, with 15 nm diameter x 60 nm length particles and volume fraction of 0.03. Simulation set (D) was run for film thickness of 100 nm, with 15 nm diameter x 90 nm length particles and volume fraction of 0.05. Simulation set (E) was run for film thickness of 50 nm, with 5 nm diameter x 5 nm length particles and volume fraction of 0.01. The results showed minimal variability between repeat runs (*Figure 4*).

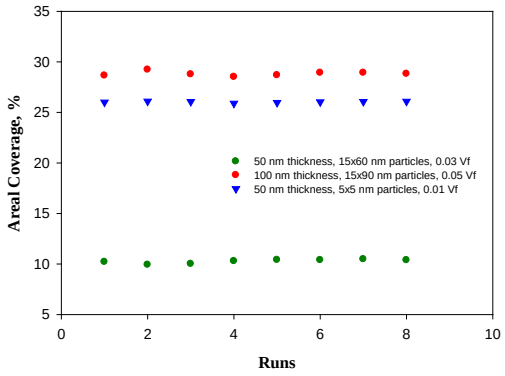

FIGURE 4. Analysis of replicability of numerical results.

Effect of Volume Fraction

The effect of volume fraction was studied through two sets of numerical simulations. The first set involved running the simulation at various volume fractions with the particle diameter, *d*, ranging from 5 to 15 nm. Particle aspect ratio, *r*, and film thickness in all the simulations in this set were kept constant at 2 and 100 nm, respectively. Analysis of the results showed that the area covered in the projected 2D visualization increases with an increase in volume fraction as shown in *Figure 5*. Additionally, the analysis also showed that smaller particles provide higher areal coverage.

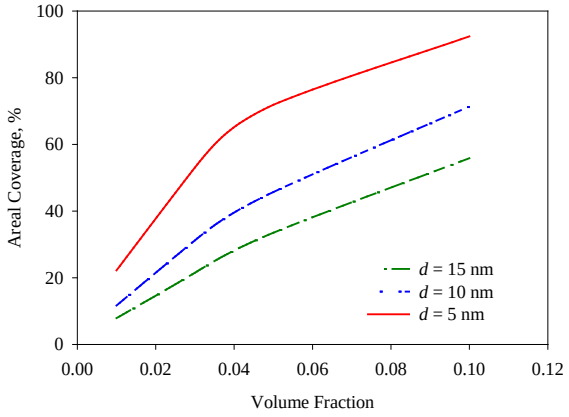

FIGURE 5. Effect of volume fraction and diameter of UV particles on area covered (particle aspect ratio = 2, film thickness = 100 nm).

The second set of numerical simulations involved running the simulations at various volume fractions, however, unlike the first set, the particle diameter was kept constant at 10 nm, and particle length, *L*, was varied from 10 nm to 60 nm. The film thickness in all the simulations was kept constant at 100 nm. In addition to showing higher areal coverage with increasing particle volume fraction, the results (*Figure 6*) also showed that increase in particle length resulted in higher areal coverage. In the case of particles with 10 nm diameter, areal coverage tended to reach its maximum at about 0.25 volume fraction.

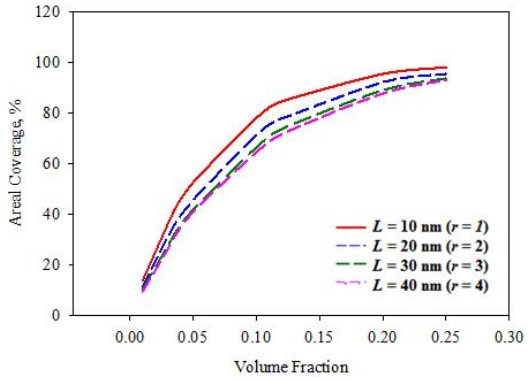

FIGURE 6. Effect of volume fraction and aspect ratio, r, of UV particles on area covered (particle diameter = 10 nm, film thickness = 100 nm).

The higher areal coverage with increasing volume fraction can be explained by higher number of particles, *N* (Eq. (1)) in the matrix. Higher number of particles due to higher volume fraction results in higher surface area which explains the increase in areal coverage as seen in the 2D visualization of the projected area (*Figure 7*).

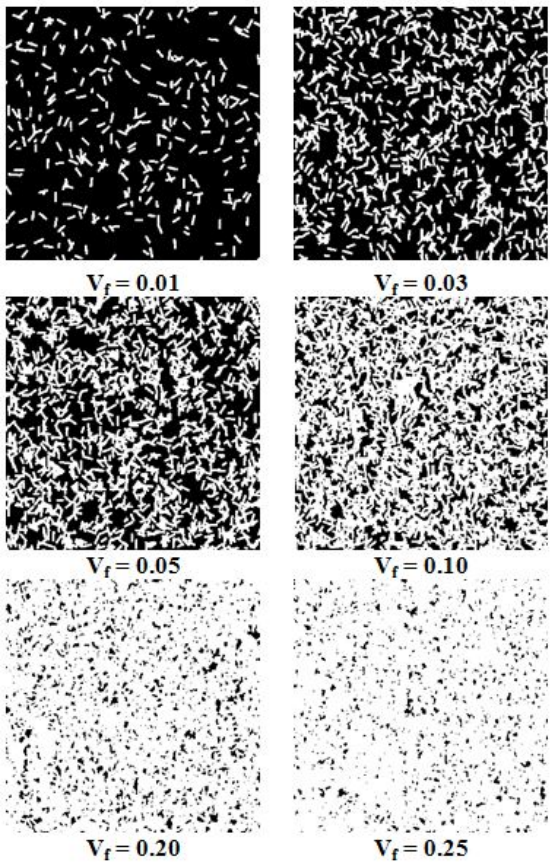

FIGURE 7. 2D visualization of 100 nm thick films containing 10 nm x 40 nm particles with different volume fractions.

Effect of Particle Length

To understand the influence of particle length on projected area covered, simulations were run with particles of various lengths such that the aspect ratio ranged from 1 to 6. The volume fraction was varied from 0.01 to 0.05, while the film thickness was kept constant at 100 nm. *Figure 8* and *Figure 9* show the results for particle diameter 5 nm and 10 nm, respectively. The areal coverage was found to decrease with an increase in particle length as also seen in *Figure 6.*

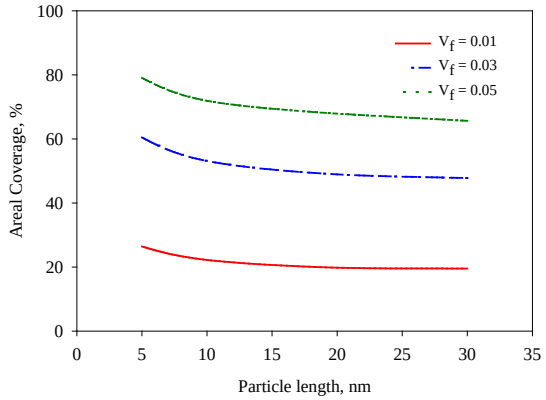

FIGURE 8. Effect of particle length on areal coverage (particle diameter = 5 nm).

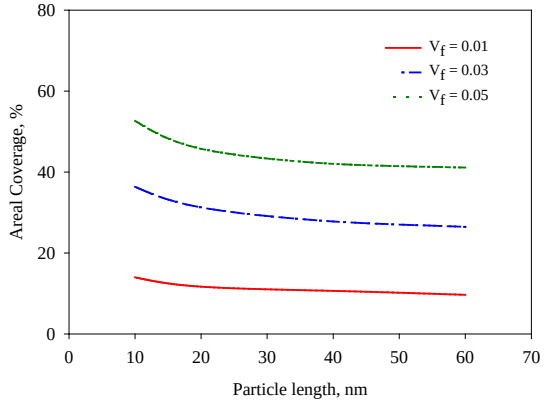

FIGURE 9. Effect of particle length on areal coverage (particle diameter = 10 nm).

For a given volume fraction and particle diameter, increase in particle length results in fewer number of particles (Eq. (1)) with lower surface area which results in lower areal coverage as shown in *Figure 10.*

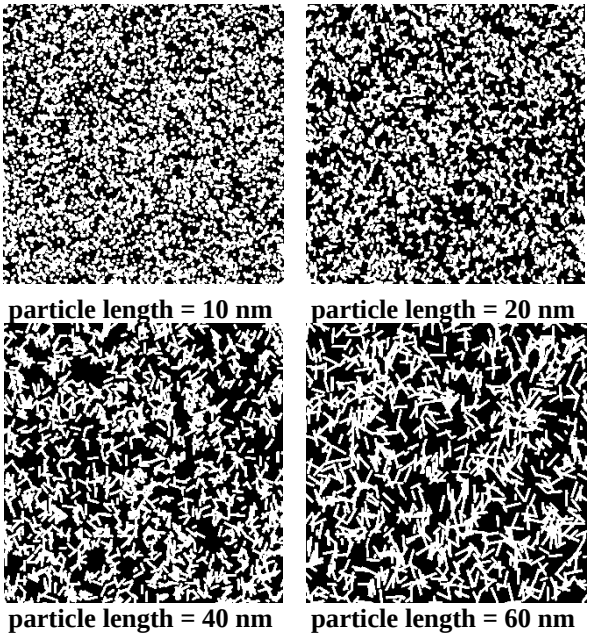

FIGURE 10. 2D visualization of 10 nm diameter nanoparticles with different particle length (volume fraction = 0.05).

Effect of Particle Diameter

To study the effect of particle diameter on the areal coverage, simulations were run with particle diameter ranging from 5 nm to 15 nm. In order to understand the interaction between particle diameter and volume fraction, the simulations were run at 4 levels of volume fraction ranging from 0.01 to 0.10. Film thickness and aspect ratio in all the simulations were kept constant at 200 nm and 4, respectively. The results are plotted in *Figure 11*. The figure shows that for all volume fraction levels, areal coverage decreases when larger diameter particles are used. The 2D visualization of films with different particle diameters is shown in *Figure 12*.

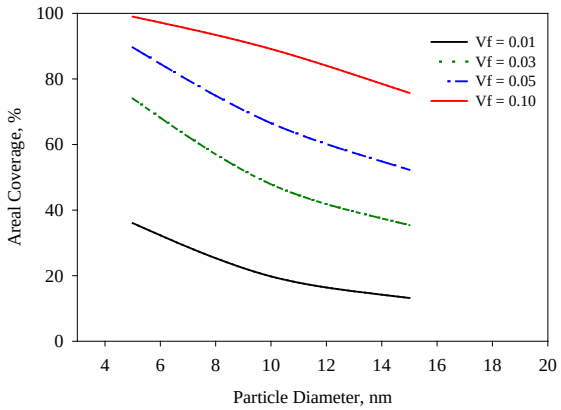

FIGURE 11. Effect of particle diameter at various levels of particle volume fractions (film thickness = 200 nm and particle aspect ratio = 4).

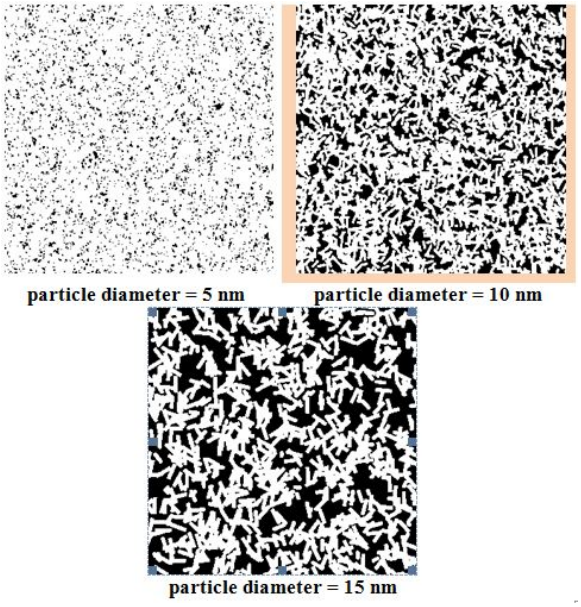

FIGURE 12. 2D visualization of films with different particle diameter (volume fraction = 0.05, particle aspect ratio = 4).

Effect of Film Thickness

To study the effect of film thickness on the areal coverage of the nanoparticles, two groups of simulations were run with film thickness ranging from 50 nm to 800 nm. In the first group, the particle volume fraction was varied from 0.02 to 0.10, while the particle diameter and particle length were kept constant at 10 nm and 40 nm, respectively (or r = 4). The results shown in *Figure 13* exhibited an exponential increase in areal coverage with increasing film thickness. The steepest increase was seen when the volume fraction was set to 0.10 where almost 100% coverage is achieved for film thickness of 400 nm.

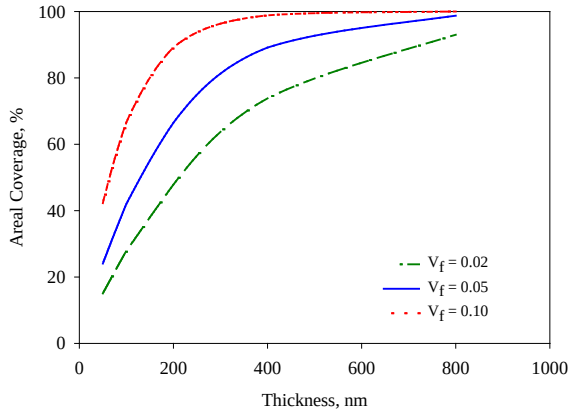

FIGURE 13. Effect of film thickness on areal coverage (particle diameter = 10 nm, particle length = 40 nm).

In the second group, the particle diameter was varied from 5 nm to 15 nm while the volume fraction and aspect ratio were set constant at 0.03 and 4, respectively. The results plotted in *Figure 14* show a significant increase in areal coverage with increasing thickness. The steepest increase in areal coverage was seen in the case of particles with 5 nm diameter with the coverage reaching 100% at a smaller film thickness compared to those in the case of larger diameter particles.

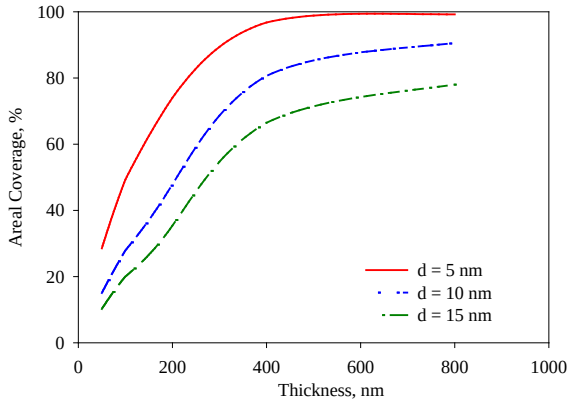

FIGURE 14. Effect of film thickness on areal coverage (volume fraction = 0.03, particles aspect ratio = 4).

The effect of the thickness exhibited a significant trend in that the area covered approaches 100% as the thickness increased. As mentioned earlier, the results are very useful in determining the least film thickness that provides maximum areal coverage. 2D visualization of nanoparticles in films with different thicknesses is shown in *Figure 15*.

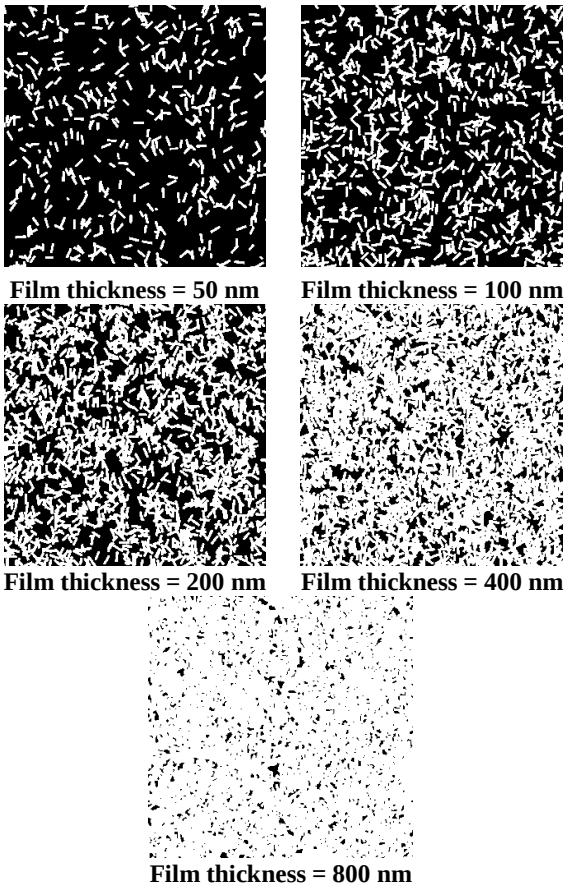

FIGURE 15. 2D visualization of nanoparticles in films with different thicknesses (volume fraction = 0.03, particle diameter ratio = 10, particle length = 40 nm).

Effect of Aspect Ratio

To study the effect of aspect ratio, particle volume fraction in the matrix and number of particles were kept constant. Particle length, and particle diameter were calculated for the desired values of aspect ratio based on the following Eq. (3) – Eq. (5).

$$\frac{V_f V_c}{N} = \frac{\pi}{4} d^2 L \tag{3}$$

$$L = rd \tag{4}$$

Where
V_f = particle volume fraction
V_c = total volume of the computational region
N = number of particles
L = particle length
d = particle diameter
r = particle aspect ratio

Substituting Eq. (4) into Eq. (3), Eq.(5) was obtained that allowed the calculation of particle diameter. Then, particle length was obtained from Eq. (4).

$$d = \left[\frac{4 V_f V_c}{N \pi r}\right]^{1/3} \tag{5}$$

Using Eq. (5), a finer diameter range (8.3 nm – 15.0 nm) and a courser diameter range (22.0 nm to 40.0 nm) were obtained for analysis of particle aspect ratios.

The results of the simulations run at various film thicknesses and volume fractions are included in *Tables I and II.*

TABLE I. Effect of aspect ratio and volume fraction on area covered by UV nanoparticles.

Particle diameter (*d*), nm	Particle length (*L*), nm	Particle Aspect Ratio (*r*)	Volume fraction, V_f = 0.02	Volume fraction, V_f = 0.05	Volume fraction, V_f = 0.10
			Area covered,%	Area covered, %	Area covered, %
15.0	15.0	1	32.65	63.54	86.17
11.9	23.8	2	33.70	64.41	87.43
10.4	31.2	3	35.04	66.94	87.02
9.5	37.8	4	37.24	69.03	90.55
8.8	43.9	5	38.42	71.07	91.51
8.3	49.5	6	40.03	72.17	91.97
Computational region dimensions: 1000 nm x 1000 nm x 200 nm					

TABLE II. Effect of aspect ratio and volume fraction on area covered by UV nanoparticles.

Particle diameter (*d*), nm	Particle length (*L*), nm	Particle Aspect Ratio (*r*)	Volume fraction, V_f = 0.05	Particle diameter (*d*), nm	Particle length (*L*), nm	Particle Aspect Ratio (*r*)	Volume fraction, V_f = 0.02
			Area covered,%				Area covered,%
40.0	40.0	1	52.68	15.0	15.0	1	63.03
31.8	63.5	2	53.13	11.9	23.8	2	63.92
27.7	83.2	3	54.17	10.4	31.2	3	66.94
25.2	100.8	4	57.50	9.5	37.8	4	69.35
23.4	117.0	5	57.70	8.8	43.9	5	71.27
22.0	132.1	6	60.42	8.3	49.5	6	72.65
Computational region dimensions: 1000 nm x 1000 nm x 200 nm				Computational region dimensions: 1000 nm x 1000 nm x 500 nm			

The results plotted in *Figure 16* show that increase in particle aspect ratio results in a small increases in areal coverage at all three levels of volume fraction (0.02, 0.05, and 0.10). The increase in areal coverage is small irrespective of the film thickness and particle diameter range as shown in *Figure 17* and *Figure 18*, respectively.

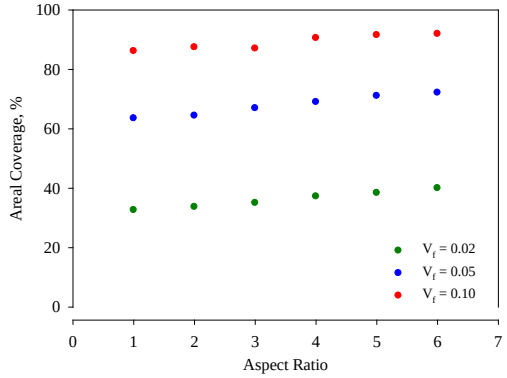

FIGURE 16. Effect of aspect ratio on areal coverage at various volume fractions (particle diameter range 8.3 nm – 15.0 nm, film thickness = 200 nm).

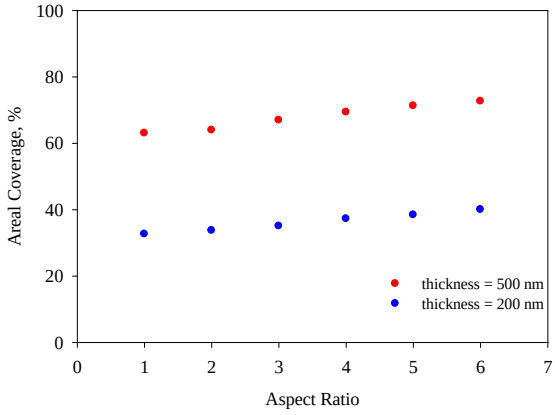

FIGURE 17. Effect of aspect ratio on areal coverage (particle diameter range 8.3 nm – 15.0 nm, volume fraction = 0.02).

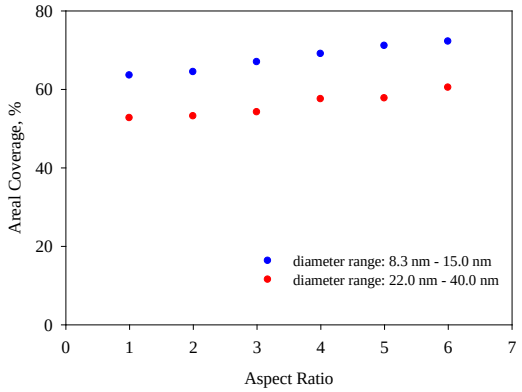

FIGURE 18. Effect of aspect ratio on areal coverage (volume fraction = 0.02, film thickness = 200 nm).

An increase in the aspect ratio from 1 to 6 is associated with around two-fold decrease in particle diameter and around three-fold increase in the particle length (*Table I* and *Table II*). An overall increase in the areal coverage as the aspect ratio increases even though particle diameter and particle length have opposing influence on areal coverage, indicates a stronger influence of particle diameter on the areal coverage as compared to the influence of particle length.

Model Verification

To verify the model experimentally, low-density polyethylene (LDPE) was compounded with 5% and 10% by weight of cylindrical TiO_2 nanoparticles of 10 nm diameter × 40 nm length (as specified by the supplier). Pellets of the compounded polymer were

microtomed into three thicknesses (100 nm, 150 nm, and 200 nm). Due to difficulty in microtoming the LDPE compounded with 5% nanoparticles were sliced into two thicknesses 100 nm and 200 nm. Three transmission electron microscope (TEM) images were taken for each sample setting. One TEM image of each sample setting is shown in *Figure 19* and *Figure 20*. As seen in the TEM images, the nanoparticles appear to be agglomerated (black or dark spots).

TEM images were processed in ImageJ using greyscale thresholding and image inversion tools to obtain black and white images. The processed images corresponding to the TEM images shown in *Figure 19* and *Figure 20* are shown in *Figures 21-25* with the white areas representing nanoparticles. To validate the computational model, 2D visualization images were generated by the model with same conditions as the TEM images (volume fraction was calculated from weight add-on %, film thickness and particles size). The experimental results of area covered by nanoparticles were compared to the theoretical results generated by the model.

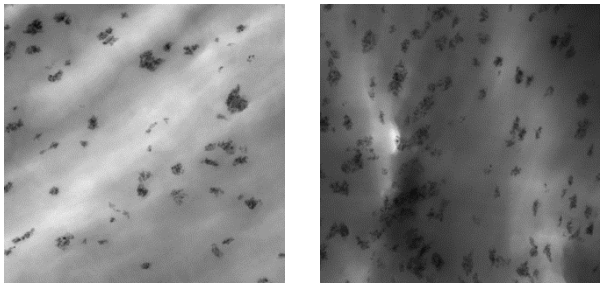

a b

FIGURE 19. TEM images for LDPE with 5% TiO_2 by weight (material thickness: (a) 100 nm (b) 200 nm).

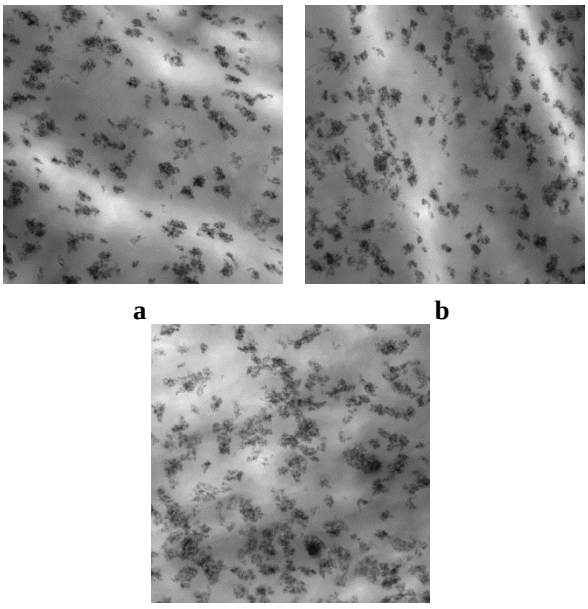

a **b**

c

FIGURE 20. TEM images of LDPE Pellet with 10% TiO_2 by weight (Material thickness: (a) 100 nm (b) 150 nm (c) 200 nm).

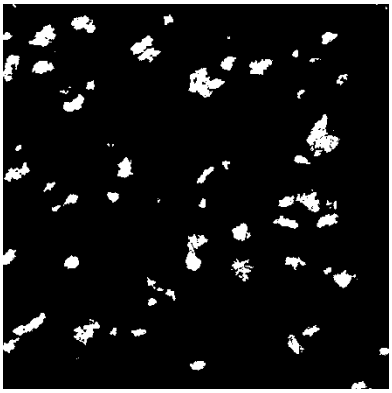

FIGURE 21. TEM image after processing using ImageJ (5% TiO_2 and thickness 100 nm).

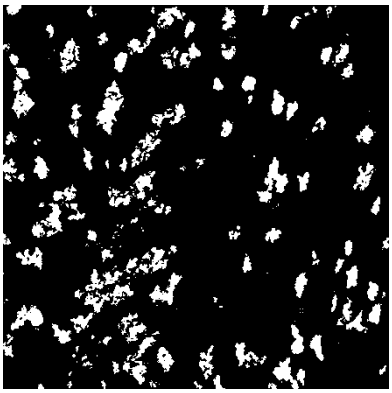

FIGURE 22. TEM image after processing using ImageJ (5% TiO_2 and thickness 200 nm).

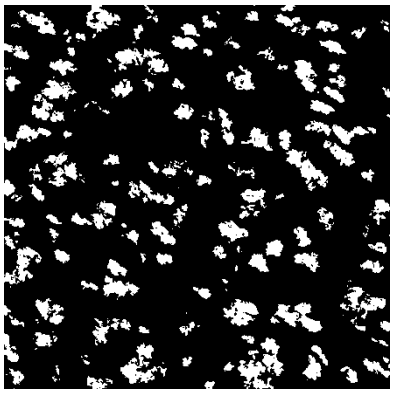

FIGURE 23. TEM image after processing using ImageJ (10% TiO_2 and thickness 100 nm).

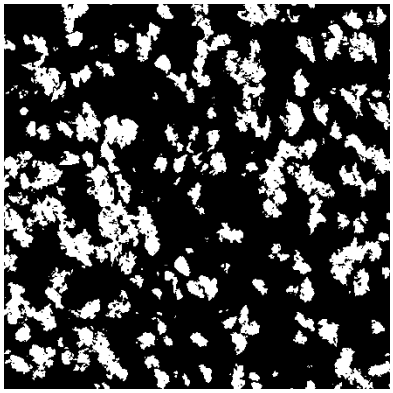

FIGURE 24. TEM image after processing using ImageJ (10% TiO_2 and thickness 150 nm).

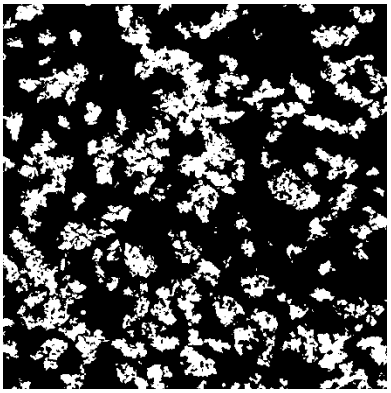

FIGURE 25. TEM image after processing using ImageJ (10% TiO_2 and thickness 200 nm).

Figure 26 and *Figure 27* show the effect of UV protective film thickness on area covered by TiO_2 nanoparticles at 5% add-on weight (V_f = 0.020) and 10% add-on weight (V_f = 0.092) respectively. Theoretical and experimental results agree in the trend showing higher areal coverage in the case of thicker film.

Figure 28 and *Figure 29* show the effect of add-on weight of UV blocker (TiO_2) particles on area covered in films of thicknesses of 100 nm and 200 nm, respectively. Again, the trends seen in theoretical and experimental results were in agreement.

As seen from *Figure 28* and *Figure 29* theoretical values of the area covered are higher than the experimental values. This is due to the agglomeration of TiO_2 particles seen in the TEM images which lowers the specific area of TiO_2 particles. The agglomerations are due to the strong Van der Waals force of attraction between the nanoparticles resulting from the high surface area of nanoparticles [18-19].

Both process parameters and polymer properties affect the dispersion of nanoparticles in the polymer matrix during compounding. More agglomeration tends to occur in case of higher polymer viscosity [20]. Shear rate during compounding also affects the dispersion of particles. Increasing shear rate has been shown to reduce agglomeration in polymer melt [21]. In general, low polymer viscosity, high stirring rate, sonication and use of suitable surfactant can lead to reduction in agglomeration.

The model represents the ideal case of random distribution of fully dispersed nanoparticles in the polymer matrix. The model has been developed as a tool to benchmark areal coverage which can be used in the development of UV protective sheaths and films.

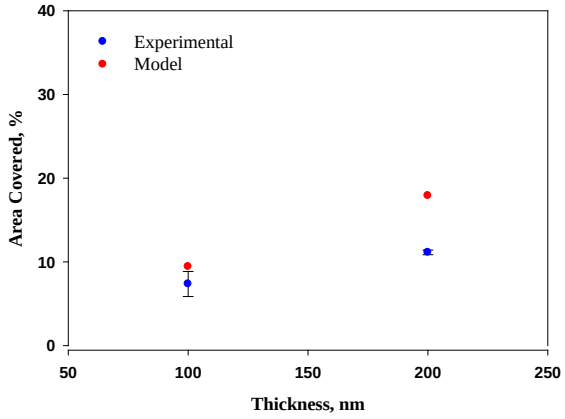

FIGURE 26. Effect of layer thickness on area covered by TiO_2 nanoparticles (5% add-on weight).

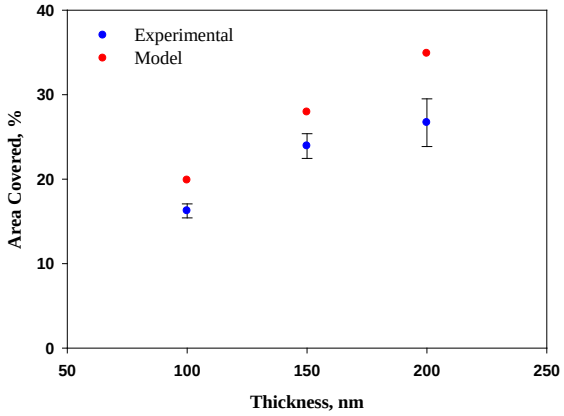

FIGURE 27. Effect of layer thickness on area covered by TiO_2 nanoparticles (10% add-on weight).

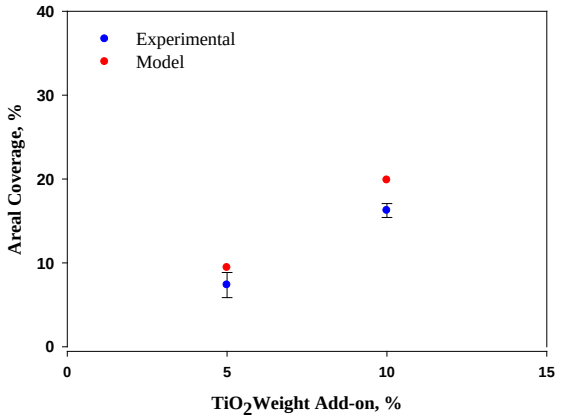

FIGURE 28. Effect of TiO_2 add-on weight on area covered (100 nm film thickness).

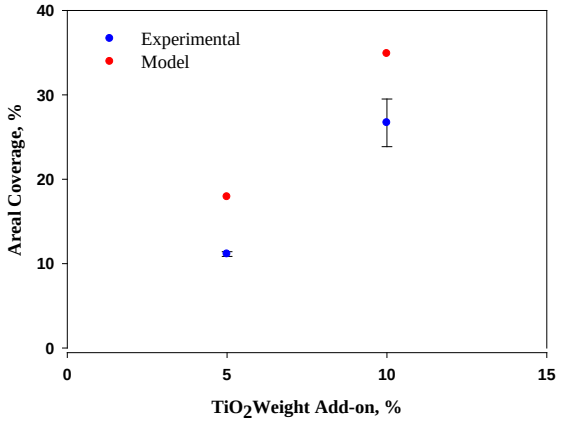

FIGURE 29. Effect of TiO_2 add-on weight on area covered (200 nm film thickness).

CONCLUSION

An idealized computational model was developed that predicts the level of UV protection provided by polymeric sheath containing cylindrical shape nanoparticles. The input parameters of the model are particle size, particle volume fraction, aspect ratio, and the polymeric film thickness. The outputs of the model are 3D visualization of the particles distribution in the computational region and 2D visualization of the particles projected on a horizontal plane. 2D visualizations were used to study the influence of the input parameters (particle diameter, particle length, aspect ratio, volume fraction, and film thickness) on the projected area covered by the UV inhibiting nanoparticles. The numerical results indicate that the projected area increased with an increase in nanoparticles' volume fraction, increase in film thickness and reduction in particle length. Increase of the aspect ratio (which was changed by keeping the number of particles and particle volume fraction unchanged) caused a small increase to the area covered by the nanoparticles. The numerical results reveal that for a given particle size and volume fraction there is an optimum layer thickness that achieves maximum protection (almost 100% projected area). Any further increase in thickness beyond the optimum value would add extra weight and cost with no improvements in the UV protection.

The trends seen in numerical and experimental results were in agreement, however, the model over predicts the areal coverage. This is attributed to the tendency of nanoparticles to agglomerate due to the high Van der Waals force of attraction. The model provides areal coverage values for ideal particle dispersion, and therefore, it can be used to evaluate experimental techniques needed to overcome the nanoparticles agglomeration issue.

ACKNOWLEDGMENT

This work is funded by the Government of Egypt (under the channel program) and the State of North Carolina, USA. The research is also funded in part by NASA, Balloon Research and Development Laboratory (BRDL) (Grant Number NNXlOAE26G). We would like to extend our thanks to Mr. Steven Chall of RENCI at North Carolina State University for helping with the VTK programming.

REFERENCES

[1] Ammala, A.; Hill, A.J.;Meakin, P.;Pas,S.J; Turney, T.W.; Degradation Studies of Polyolefins Incorporating Transparent Nanoparticles Zinc Oxide UV Stabilizers; Journal of Nanoparticles Research 2002, 4,167-174.

[2] Walsh, P. J.; Hu, X.; Cunniff, P.; Lesser A. J.; Environmental Effects on Poly-p-phenylenebenzobisoxazoleFibers. I. Mechanisms of Degradation, Journal of Applied Polymer Science2006, 102, 3517–3525.

[3] Zhang, H.; Zhang J.; Chen J.; Hab X.; Wang S.; Feng X.; Guo Y.; Effect of Solar UV Irradiation on The Tensile Properties And Structure of PPTA Fiber, Polymer Degradation And Stability 2006, 91,2761-2767.

[4] Walsh, P. J.; Hu, X.; Cunniff, P.; Lesser A. J.; Environmental Effects on Poly-P-Phenylenebenzobisoxazole Fibers. II Attempts at Stabilization, Journal of Applied Polymer Science 2006, 102, 3819–3829.

[5] Xing. Y.; Ding, X.; UV Photo-Stabilization of Tetrabutyl-Titanate For Aramid Fiber Via Sol-Gel Surface Modification, Journal of Applied Polymer Science 2007, 103,3113-3119.

[6] Chen, X.; Dong, W. Z.; Liao, Z. Fu.; Mai, Y. L.; Zhang, M. Q.; Role of Anatase And Rutile TiO_2 Nanoparticles in Photo-Oxidation of Polyurethane; Polymer Testing 2007, 26,202-208.

[7] Gupta, A.;2005, Improving UV Resistance of High Strength Fibers, M.S. thesis, North Carolina State University, Raleigh, NC, 2005 (Under direction of Abdel-Fattah M. Seyam and Gary N. Mock).

[8] Hassanin, A.; Improving UV Resistance of High Performance Fibers, PhD North Carolina State University, Raleigh, NC, 2011 (Under direction of Dr: Abdel-Fattah M. Seyam).

[9] Xin, J.H.;Daud, W.A.; Kong, Y.Y.; A New Approach To UV-Blocking Treatment For Cotton Fabrics, Textile Research Journal 2004,74, 97-100.

[10] Riedel, J.H.; Hocker, H.; Multifunctional Polymeric UV Absorbers for Photostablization of Wool, Textile Research Journal 1996, 66,684-689.

[11] Wypych, G.; Handbook of Material Weathering, (2nd Edition), ChemTec Publishing: 1995, Online version available at:http://www.knovel.com/web/portal/browse/display?_EXT_KNOVEL_DISPLAY_bookid=318&VerticalID=0

[12] Yang, H.; Zhu S.; Pan N.; Studying the Mechanisms of Titanium Dioxide as Ultraviolet-Blocking Additive for Films and Fabrics by an Improved Scheme; Journal of Applied Polymer Science 2004, 92, 3201–3210.

[13] Katangur, P.; Patra P.K.; Nanostructured Ultraviolet Resistant Polymer Coating, Polymer Degradation And Stability2006, 91, 2437-2442

[14] Hearle, J. W.; High Performance Fibers; Wood head Publishing Ltd: Cambridge, 2001.

[15] Moore, R.A.; Weigmann H.D.; Dye Ability Of Nomex Aramid Yarn, Textile Research Journal 1986, 56,254-260.

[16] Yamamotoa, A.; Atsutaa, S.; Kanemitsua Y.; Fabrication and photoluminescence studies of ZnOnanocrystals dispersed in glass films, Journal of Luminescence 2005, 112, 69-172.

[17] Vallabh, R.; Ducoste, j; Seyam, A; Bank-Lee, P; Modeling Tortuosity in Thin Fibrous Media using Compuational Fluid Dynamics, Journal of Porous Media, 2011, 14, 791-804.

[18] Sauter, C.; Emin, M.; Schuchmann, H.; Tavman, S.; Influence of hydrostatic pressure and sound amplitude on the ultrasound induced dispersion and de-agglomeration of nanoparticles; UltrasonicsSonochemistry2008, 15. 517-523.

[19] Qiang, L.; Nanoparticle dispersions in polymers: Homopolymer versus block copolymer, MI, USA, University of Minnesota, PhD thesis, 2008 (Under supervision of Bates Frank, Francis Lorrian).

[20] Kotsilkava, R.; Thermoset nanocomposites for engineering application; Smithers Rapra Technology Limited: Shawbury 2007.

[21] Kalra, V.; Escobedo, F.; Jooa, Y.; Effect of shear on nanoparticle dispersion in polymer melts: A coarse-grained molecular dynamics study; Journal of Chemical Physics2010, 132, 1-11.

AUTHORS' ADDRESSES
Abdelfattah Mohamed Seyam, PhD
Rahul Vallabh, PhD
Ahmed H. Hassanin, PhD
North Carolina State University
2401 Research Drive
Raleigh, NC 27695-8301
UNITED STATES